Journal of
MATERIALS RESEARCH



# Tensile testing low density multilayers: Aluminum/titanium

D. Josell
*National Institute of Standards and Technology, Gaithersburg, Maryland 20899-0001*

D. van Heerden
*Johns Hopkins University, Baltimore, Maryland 21218-2680*

D. Read
*National Institute of Standards and Technology, Boulder, Colorado 80302*

J. Bonevich
*National Institute of Standards and Technology, Gaithersburg, Maryland 20899-0001*

D. Shechtman
*Technion, Haifa, Israel*

(Received 23 October 1997; accepted 27 March 1998)

Yield stresses, ultimate tensile strengths, and specific strengths of aluminum/titanium multilayer thin films are determined from the results of uniaxial tensile tests. The plasticity in the stress-strain curves, the nature of the fracture surfaces, and the relationship of the yield stress and the bilayer thickness are discussed. Properties are compared with those of other multilayer materials published in the literature.

## I. INTRODUCTION

Mechanical properties of multilayer thin films are most often obtained by nanoindentation (for a recent review see Ref. 1. Few studies obtain tensile properties of these materials from stress-strain and fracture behavior. Most can be found in recent survey articles.[1,2] Of the studies, many are concerned with the Cu/Ni system[3–6] Also see Ref. 7 for theory.

The Al/Ti multilayer system was selected for this study of tensile properties because of the low densities of the constituent materials Al (2.7 $g \cdot cm^{-3}$) and Ti (4.5 $g \cdot cm^{-3}$). The density of the material studied was reduced to a nominal value of 3.3 $g \cdot cm^{-3}$ by depositing Al layers approximately twice the thickness of the Ti layers. The results of tensile tests conducted on these materials are analyzed and compared to published properties of both high strength alloys and other multilayer systems.

In the only published study of the tensile properties of Al-based metal/metal multilayer materials of which the authors are aware, Lehoczky[8,9] studied the fracture of Al/Cu and Al/Ag multilayers. His experiments on Al/Cu multilayers with equally thick layers indicated that the ultimate tensile strength (UTS) of these materials reached a plateau, at approximately 700 MPa, for bilayer thickness $\Lambda$ less than 140 nm. For $\Lambda > 140$ nm, the tensile strength varied as the inverse square root of the layer thickness. Lehoczky argued that, in a manner analogous to the Hall–Petch dependence of yielding on grain size, the large $\Lambda$ behavior of the UTS was associated with dislocation pileups in the Al required to raise local stresses and nucleate cleavage cracks. From the stress-strain curves, Lehoczky also found that the tensile yield stress was nearly constant for $\Lambda$ less than approximately 140 nm (Al/Cu) and 460 nm (Al/Ag).[9] In contrast, from the results of nanohardness tests conducted on Al/Ti multilayers, Ahuja and Frasier[10] concluded that the hardness was proportional to the inverse square root of the bilayer thickness for the 1.7 to 63 nm thickness range examined.

In this study the tensile properties of 6–10 $\mu$m thick Al/Ti tensile specimens have been evaluated. Because the measured tensile properties of thin films can depend on film geometry, i.e., gauge length, gauge width, and film thickness, stress-strain curves were also obtained on one set of Al/Ti multilayer films using a second tensile geometry and testing technique.

## II. CHARACTERIZATION

### A. Specimen geometry

All the specimens were produced using shuttered electron beam evaporation sources in a vacuum of the order $10^{-5}$ Pa ($10^{-7}$ Torr). The majority of the tensile tests were conducted on individual freestanding multilayer thin films between 5 and 10 $\mu$m thick, 10 mm wide, and between 10 mm and 25 mm long (“large” gauge). Freestanding specimens were obtained by dissolving a sacrificial layer of either Cu or NaCl (evaporated onto the substrate prior to deposition of the multilayers) in dilute nitric acid or water, respectively. Freestanding multilayers with bilayer thicknesses $\Lambda = 13$, 40, and 90 nm (nominal Al : Ti thickness ratio 2 : 1) were prepared. Multilayers with $\Lambda = 20$ nm (nominal 16 : 7 Al : Ti

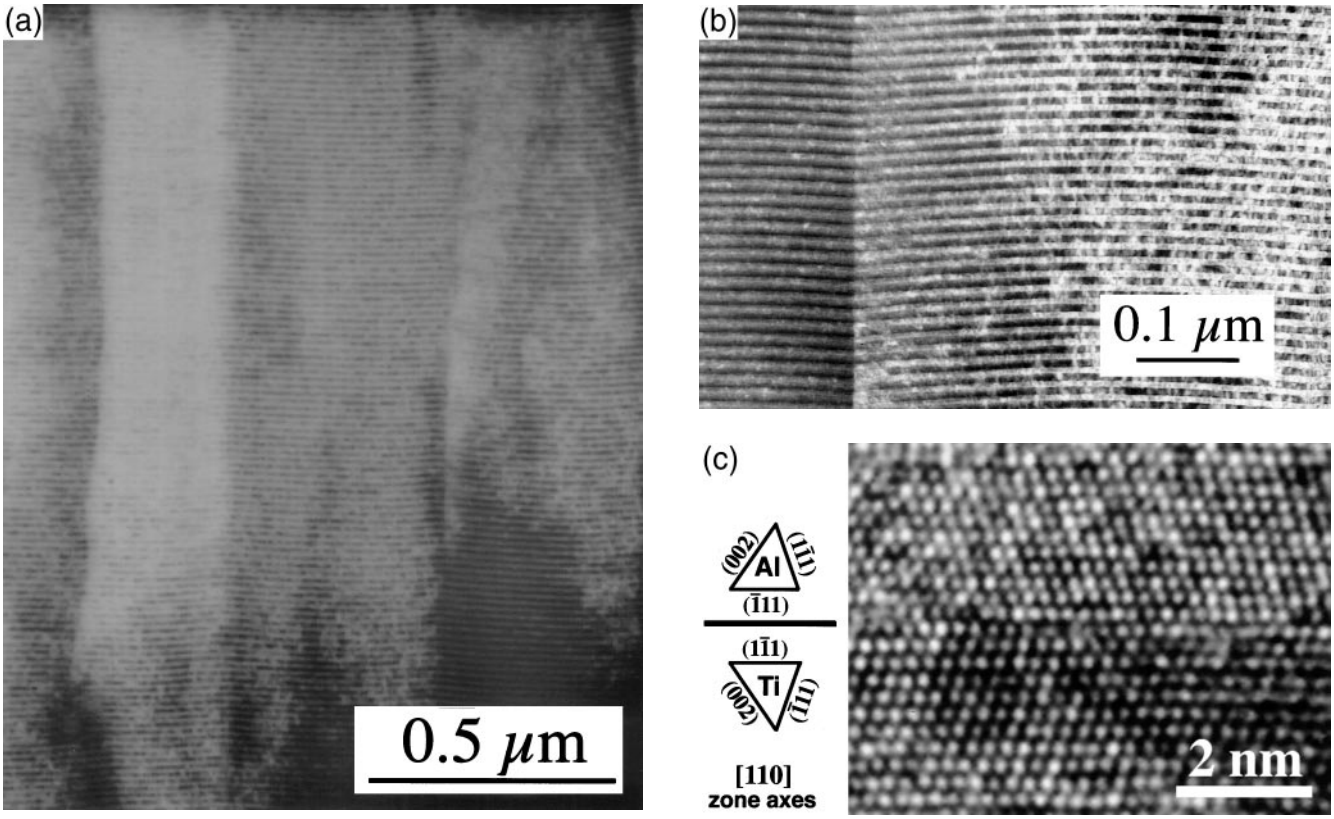


FIG. 1. (a) Al/Ti multilayers are composed of columnar grains (TEM, bright field). (b) Grain boundary (TEM, bright field). (c) The interface between Al and Ti layers is atomically sharp (high resolution TEM). Note that the Ti layer has adopted an fcc structure during preparation for cross-section TEM, creating a $\Sigma = 3$ type twin boundary (with misfit dislocations) between the layers. The characteristic planes for the fcc (110) zone axes in the layers are indicated to the left of the image.

thickness ratio) were also fabricated in two separate deposition runs. Multiple specimens of each bilayer geometry were deposited simultaneously on a water-cooled stage that prevented both intermetallic formation and grain boundary grooving induced degradation of the layered structure during deposition. The use of a cooled substrate, necessary with this system for the stated reasons, contrasts with the heated substrate used to limit defects and maximize texturing and density in several other studies.[3,5] Because of the chamber geometry and size of the specimen mask, there was some thickness and composition variation of the simultaneously fabricated specimens. The size and effect of this specimen variability on the measured properties is examined in Sec. III.

Stress-strain curves were also obtained from tensile specimens composed of either one, three, or four parallel multilayer strips each 1.26 $\mu$m thick and 0.245 mm wide with gauge lengths 0.920 mm ("small" gauge) held in a tensile frame. These tensile specimens were thinner than the "large" gauge specimens due to limitations of the test apparatus and were prepared only with bilayer thickness $\Lambda = 14$ nm (nominal Al : Ti thickness ratio 2 : 1). The small gauge specimens were deposited on a Si substrate that had previously been prepatterned with $SiO_2$. Additional patterning and etching in a solution of aqueous hydrazine at 100 °C to remove Si from beneath the gauge section of the tensile specimen were also required after deposition of the multilayer coating. Details of the general process are given in Ref. 11.

Specimen thickness was determined by scanning electron microscopy (SEM) of polished cross sections. Fracture surfaces of the tensile specimens were also examined by SEM.

### B. Specimen microstructure

The microstructure of characteristic Al/Ti multilayers as observed by transmission electron microscopy (TEM) has been published previously.[12,13] The layer growth is epitaxial with columnar "grains" extending through most of the multilayer thickness [Figs. 1(a) and 1(b)]. The width of the columnar grains is much larger than the thickness of the individual bilayers. The grains are seen by x-ray diffraction to be highly textured, with close packed (111) face-centered cubic Al and (0002) hexagonal Ti planes parallel to the interfaces between the layers. The Ti/Al interfaces are atomically sharp, with no more than one or two monolayers of mixing

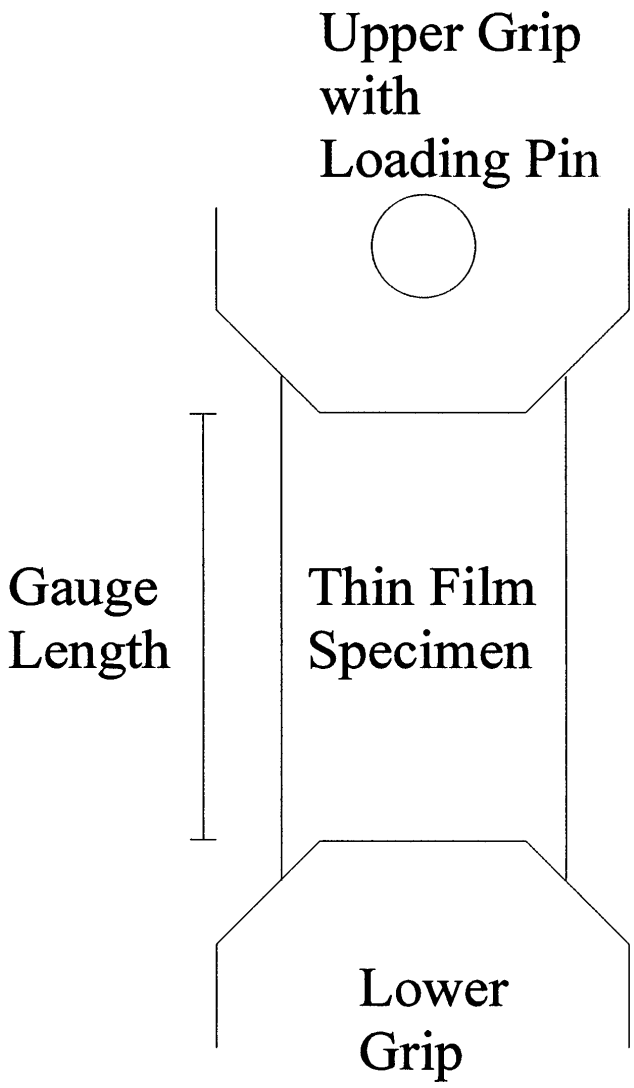


FIG. 2. A schematic of the grip geometry.

[Fig. 1(c)]. When thinned in cross section for TEM, the Ti layers transform to (111) textured face-centered cubic Ti [evident in Fig. 1(c)], the subject of previous papers.[12,13] However, in all cases, the Ti layers deposit with the equilibrium hexagonal structure, and such was the structure of the Ti layers in the multilayer tensile specimens.

### C. Mechanical properties

#### 1. Large gauge specimens

Tensile tests were carried out on the large gauge films using a conventional worm-gear driven tensile testing machine. Stainless steel tabs were glued to the ends of the multilayer films to facilitate gripping. The tabs were tapered with the tab end defining the end of the gauge length to be less wide than the width of the film (Fig. 2). The point at which the tab crossed the film edge was thus recessed from the gauge length, reducing the stress concentration where grip-induced failures had occurred in earlier tests; no failures at the grips were observed with this geometry.

The nominal 8.5 $\mu$m $s^{-1}$ and 85 $\mu$m $s^{-1}$ displacement rates imposed by the tensile machine crosshead give strain rates of approximately $3 \times 10^{-4}$ $s^{-1}$ and $3 \times 10^{-3}$ $s^{-1}$, respectively, for 2 cm long specimens. However, actual strain rates appear to have been lower than the nominal rates; Young's moduli obtained using the crosshead velocities to determine specimen strains were consistently 50–60% of the volume weighted elemental moduli. The output of two capacitive extensometers, used with several specimens to directly measure the displacement of the crosshead attached to the specimen, yielded similarly low values. Specimen strain, determined using both methods, is thus considered to be ill-measured.

The (engineering) stress in the specimen was determined from the force measured by a calibrated load cell in series with the specimen divided by the initial cross-sectional area of the specimen.

#### 2. Small gauge specimens

Tensile tests on the small gauge specimens were conducted simultaneously on the one or multiple ("multi") sample strips contained in a frame, straining all of the constituent strips in parallel. The measured force thus represents the sum of the forces in the individual strips. The microtensile testing rig has been described previously.[11] Speckle interferometry was used to measure the strains included in Sec. III.

## III. TENSILE TEST RESULTS

Tensile stress-strain curves for the large gauge Ti/Al specimens are shown in Fig. 3. Results for specimens that broke prior to reaching two-thirds of the yield stress (for that bilayer thickness) are not included as the delicate specimens might have been damaged during separation from the substrate or mounting. The variation of the slope (i.e., modulus) from specimen to specimen is indicative of the unreliable strain measurements. This introduces some uncertainty into the yield stresses because they are defined as the stress where the plastic strain first reaches a threshold value. However, for the threshold value of 0.01%, selected because of the limited plasticity observed, a 100% overstatement of strain results only in a 20 MPa understatement of the yield stress.

Figure 4(a) shows examples of the plastic strain versus stress obtained from the Al/Ti multilayer stress-strain curves in Fig. 3. The plastic strain for each specimen was obtained by subtracting the linear elastic strain, an extrapolated fit to the linear portion of the stress-strain curve, from the total strain. The yield stresses of all the specimens, large and small gauge, are shown in Fig. 4(b).

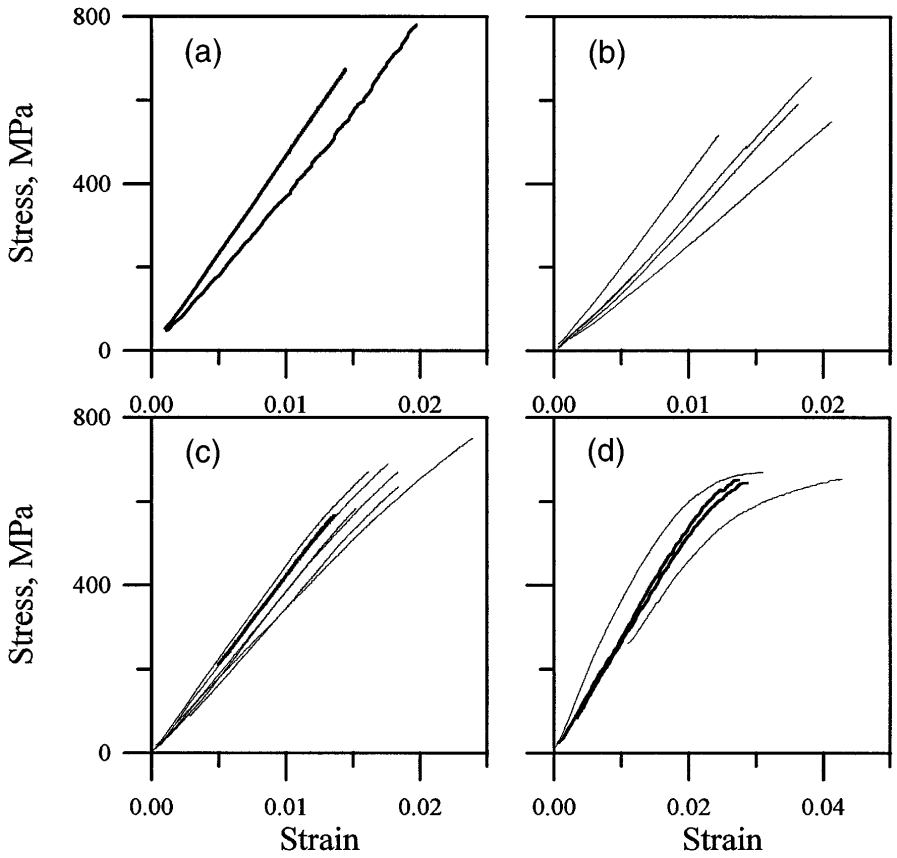


FIG. 3. Stress-strain curves for the large gauge specimens. Bilayer thickness $\Lambda$: (a) 13 nm, (b) 20 nm, (c) 40 nm, and (d) 90 nm. Curves for the specimens tested at the higher crosshead velocity are shown in bold.

Though the yield stress does increase with decreasing bilayer thickness $\Lambda$, the dependence is not as strong as the Hall–Petch type $\Lambda^{-1/2}$ dependence. The average UTS and yield stress, as well as the highest value of UTS for each group of specimens, are given in Table I.

The stress-strain curves obtained from the small gauge specimens are shown in Fig. 5. The average UTS and yield stress, as well as the highest value of UTS for each group of specimens, are also given in Table I.

The measured thickness variation noted in Table I is caused by limitations of the deposition system arising from the number of specimens that were simultaneously deposited. Because of this variation, both the thickness and average composition of each specimen were measured from cross-sectioned specimens (after the tensile tests) using an SEM and quantitative energy dispersive x-ray spectroscopy. Linear regression analysis of the data indicated that the variation of bilayer thickness within each group of films was not significantly correlated with the variation of properties obtained and that there was no statistically significant correlation with the variation of composition.

Plastic deformation prior to fracture increased with increasing bilayer thickness $\Lambda$ [Fig. 4(a)]. However, the fracture surfaces of all specimens exhibited plasticity. For the small $\Lambda$ specimens, consistent with the stress-strain curves, this plasticity was limited to the fracture surfaces themselves. Wrinkles perpendicular to the tensile direction, associated with plastic deformation, were visible on the gauge sections of only the fractured large $\Lambda$ specimens. Also, the strain rate of the tests appeared to affect the plastic behavior of the $\Lambda = 90$ nm multilayers [Fig. 3(d)], though the yield stress was unchanged.

Comparison of fracture surfaces, see Fig. 6(a), and the columnar grain structure of Ti/Al films, see Figs. 1(a) and 1(b), indicates the presence of both inter- and transgranular failure. Plan-view scanning electron micrographs of fractured large $\Lambda$ specimens [Fig. 6(b)] revealed that cracks typically initiated at more than one site, leaving behind a tortuous crack path and a number of isolated small cracks. Though less convoluted, the fracture surfaces of the small $\Lambda$ specimens contained a variety of features. Figure 7 shows features from the fracture surface of a $\Lambda = 13$ nm specimen. Though no macroscopic plastic yielding was recorded through the 674 MPa UTS, the ductile, transgranular nature of the fracture is evident in Fig. 7(a). The fine scale ductile dimples observed on the fracture surface indicate a void

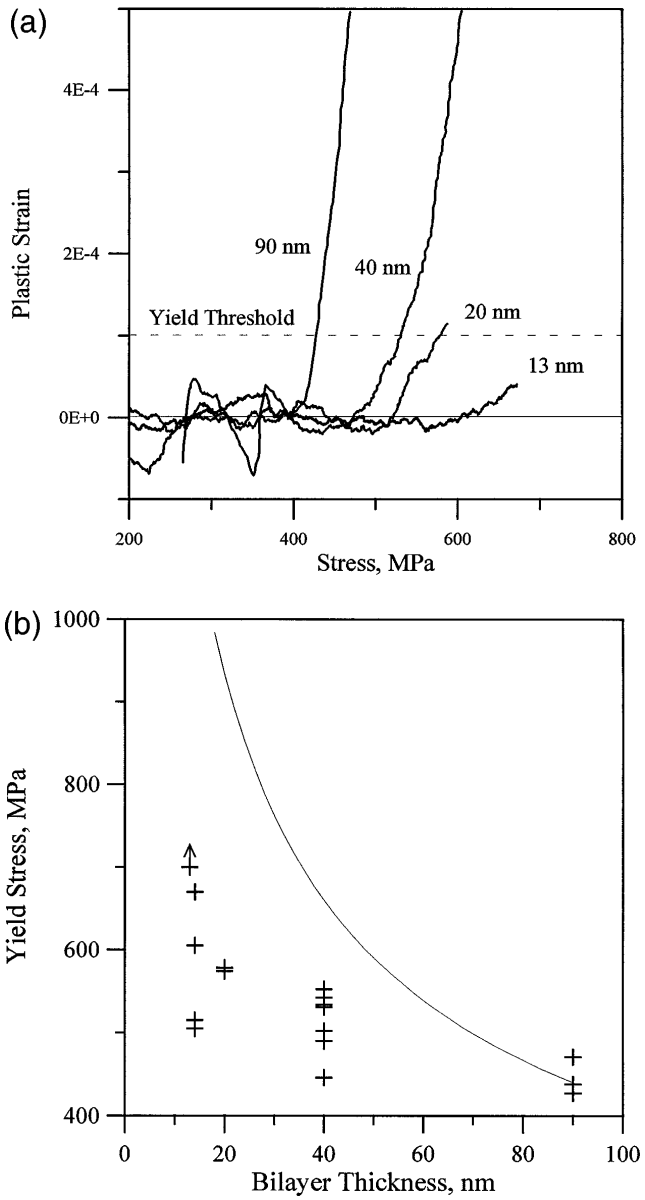


FIG. 4. (a) Plastic strain versus applied stress for one large gauge specimen of each bilayer thickness. The threshold plastic strain used to define the yield stress is indicated. (b) The dependence of the yield stress data on the bilayer thickness. A lower bound value is shown for the $\Lambda = 13$ nm specimen which failed without reaching the plastic strain threshold. A curve for yield stress proportional to $\Lambda^{-1/2}$, scaled to match at $\Lambda = 90$ nm, is also shown.

coalescence fracture mechanism. Note also the ductile "cup and cap" necking associated with an instability discussed in Sec. IV. B as well as the chevron marks expected on the fracture surface of a tensile specimen with a large width to thickness ratio. The chevron marks indicate the local crack propagation direction. Growth defects on the fracture surface are shown in Fig. 7(b), and the columnar growth morphology is evident in the region of intergranular failure shown in Fig. 7(c). The intergranular failure around the defects is consistent with weak bonding at these locations.

The $\Lambda = 20$ nm specimens were fabricated in two groups. One specimen from each group failed after yielding plastically, one from each group failed prior to yielding. As a result the average UTS is only slightly greater than the average yield stress (Table I). The two yield stresses that were obtained are nearly identical [Fig. 4(b)].

The average UTS obtained from the $\Lambda = 14$ nm small gauge multispecimens is approximately 25% higher than the value obtained from the $\Lambda = 13$ nm large gauge specimens (Table I). The average UTS of the small gauge single specimens is more than 50% higher. This increase of UTS with decreasing specimen dimension indicates the problems inherent in comparing values from specimens with different dimensions. The different UTS values of the small gauge single, small gauge multi, and large gauge specimens are believed to result from the increased probability of a given size defect in the larger specimens and the limited number of results. There is no significant difference between the yield stresses; however, the uncertainty in the data is large.

In comparison to bulk materials, 0.2% yield stresses for high strength aluminum and steel alloys are approximately 500 and 1800 MPa.[14] The 0.01 % yield stresses of the Al/Ti multilayers (Table I) are similar to, or higher than, the 0.2% yield stress for the aluminum alloy, depending on bilayer thickness. Accounting for the different densities of the materials, the 0.2% yield stresses divided by density for the alloys are 180 and 230 $\text{MPa} \cdot \text{cm}^3 \cdot \text{g}^{-1}$, respectively. The density scaled 0.01% yield stresses of the 13 and 14 nm Al/Ti multilayers fall between these values.

## IV. ANALYSIS

### A. Comparison to other tensile results

The average and highest ultimate tensile strengths are compared, where possible, with the highest values obtained from other multilayer systems in Table II. Specific strength values, UTS divided by the average density of the material, are also given in Table II. The UTS values obtained for the Al/Ti multilayers are similar to those obtained from Al/Cu multilayers by Lehoczky.[8] The specific strengths of the Al/Ti multilayers are, as a whole, significantly higher.

### B. Discussion

The Cu/Ni multilayers in Table II with 1 : 9 Cu : Ni composition, which includes the specimen with the highest UTS, were all electrodeposited using a single bath technique. Because of the single bath fabrication technique used, those multilayers contain approximately

TABLE I. Summary of tensile test results.

| Bilayer thickness (nm) | Specimen thickness ($\mu$m)[1] | Thickness ratio of Al to Ti[2] | Specimens | Yield stress[3,4] (0.01%) (MPa) | UTS average[4] (MPa) | UTS highest (MPa)[1] |
|---|---|---|---|---|---|---|
| Small gauge | | | | | | |
| 14 (Al : Ti 2 : 1) (single) | 1.25 ± 0.1 | 2.0 ± 0.25 | 2 | 593 ± 77 (2) | 990 ± 97 | 1080 |
| 14 (Al : Ti 2 : 1) (multi) | 1.25 ± 0.1 | 2.0 ± 0.25 | 2 | 555 ± 50 (2) | 788 ± 28 | 816 |
| Large gauge | | | | | | |
| 13 (Al : Ti 2 : 1) | 6.0 ± 0.2 | 1.8 ± 0.1 | 3 | >700 (0)[5] | 727 ± 53 | 780 |
| 20 (Al : Ti 16 : 7) | 9.0 ± 0.2 | 2.25 ± 0.25 | 8 | 576 ± 2 (2) | 581 ± 52 | 656 |
| 40 (Al : Ti 2 : 1) | 7.5 ± 0.4 | 1.95 ± 0.2 | 7 | 508 ± 33 (2) | 652 ± 59 | 751 |
| 90 (Al : Ti 2 : 1) | 10.1 ± 0.2 | 1.85 ± 0.15 | 4 | 445 ± 19 (3)[6] | 655 ± 9 | 670 |

[1]Measurements of the thickness (stress) for each film are certain to ±2 %. [2]The average composition of each cross-sectioned specimen, determined by quantitative energy dispersive x-ray spectroscopy, was used to determine the relative layer thicknesses. [3]The number of specimens that attained the threshold plastic strain 0.01% prior to failure is given in parenthesis. [4]The standard deviation of the data is also given. [5]The value is extrapolated from the stress-strain curve of the specimen that failed at 674 MPa and less than 0.005% plastic strain. The specimen that failed at 780 MPa exhibited anomolous stiffness increasing throughout the loading curve due to specimen realignment. [6]The yield stress from one specimen tested at the slow strain rate is not included because off-axis loading is suspected.

3 mass % Cu in the Ni layers; variation of the incorporated Cu was seen to have a substantial impact on the UTS of 100 nm bilayers.[4] Intermixing and/or possible NiO formation at the interfaces of the electrodeposited coatings were proposed as possible reasons for the substantial difference between the properties of those films and vapor deposited Cu/Ni multilayer films also shown in Table II. Multilayers deposited using vapor deposition techniques typically contain no oxides and have intermixing only at an atomic level near the interfaces.

Lehoczky noted that the UTS of his Al/Cu multilayers was approximately 100 MPa larger than the yield stress over the entire range of bilayer thickness studied.[8] This 100 MPa offset is associated with a necking instability once the thin films begin to deform plastically; this effect was also noted by Bunshah *et al.* for Cr/Cu multilayers at bilayer thicknesses for which the yield stress was less than the fracture stress.[15] Failure follows a localized gauge displacement that, though it depends on the plastic stress-strain curve for the particular specimen, should be approximately 1–10 times the specimen thickness. For Lehoczky's ~1 $\mu$m thick,

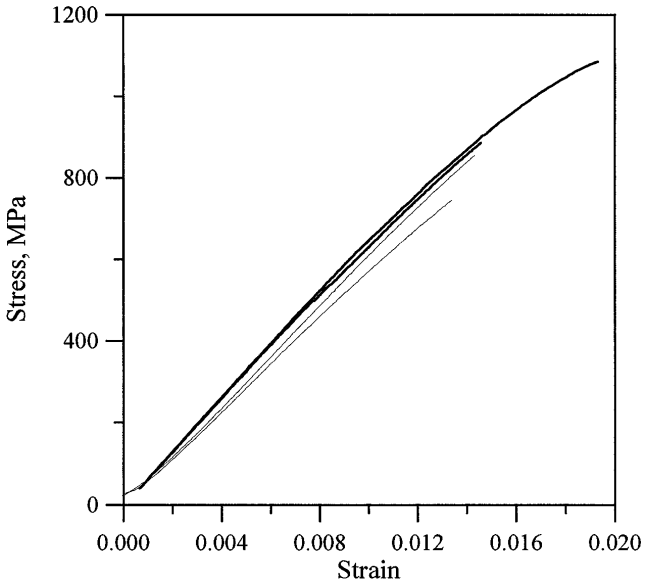


FIG. 5. Stress-strain curves for the small gauge single and multi $\Lambda$ = 14 nm specimens.

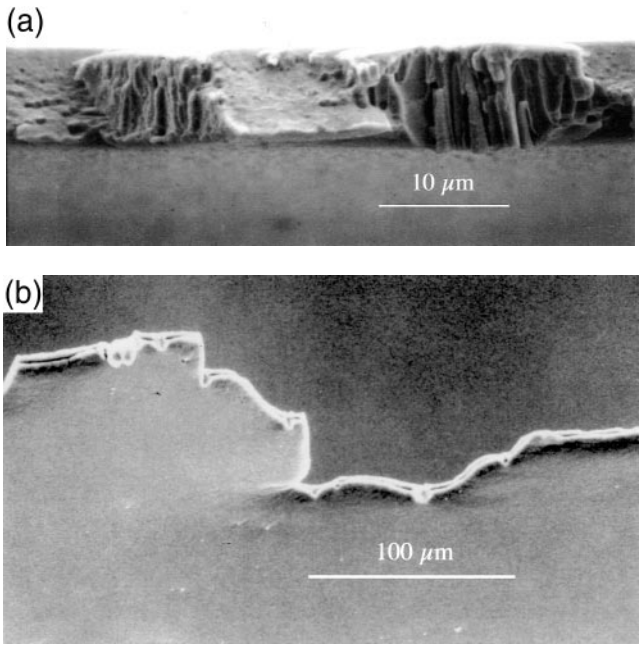


FIG. 6. Scanning electron micrographs of failed large gauge specimens: (a) cross-section view of a $\Lambda$ = 40 nm specimen fracture surface exhibiting regions of inter- and transgranular fracture; (b) plan-view of a $\Lambda$ = 90 nm specimen showing the defect controlled path of the fracture.

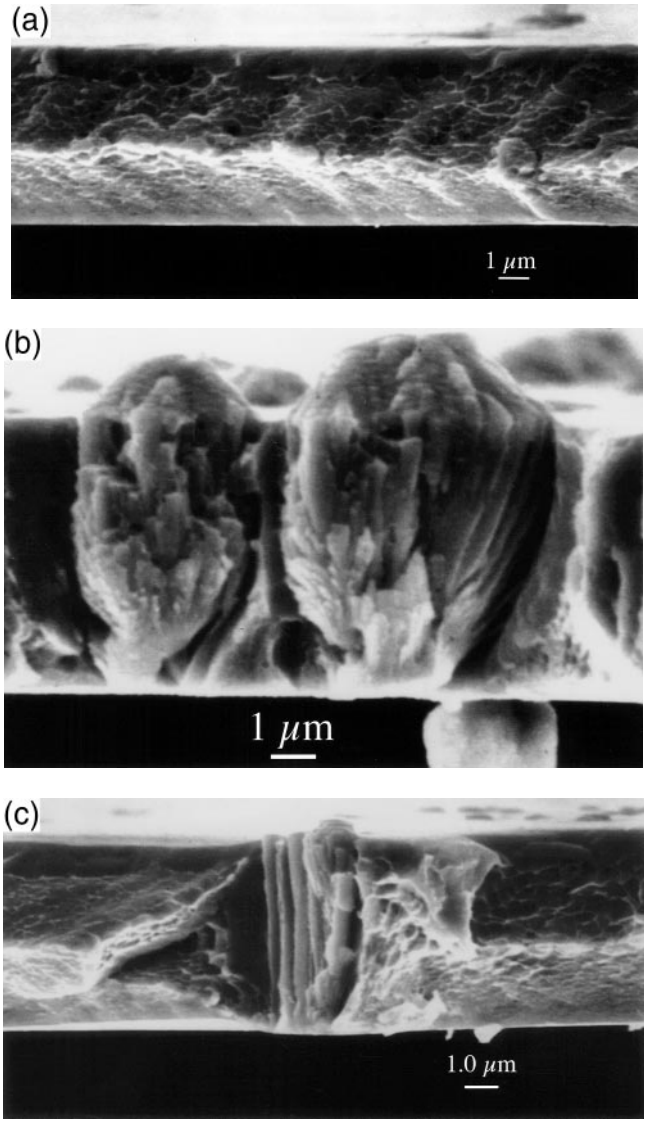


FIG. 7. SEM micrographs of features from a $\Lambda = 13$ nm fracture surface (growth direction up): (a) ductile failure by localized necking, (b) intergranular failure around two typical growth defects (dust, acquired after removal from the substrate, is visible beneath), and (c) intergranular failure around the columnar "grains" of the film.

10 mm long specimens, the strain associated with such a 10 $\mu$m displacement would be $\sim 10^{-4}$–$10^{-3}$. This is in approximate agreement with the $1-3 \times 10^{-3}$ plastic strains visible in Lehoczky's figures. The same instability induced necking rule for multilayer specimens with bulk sample dimensions like the Cu/Fe specimens of Bunshah *et al.*,[6] with length 10 mm and thickness 0.8 mm, predicts 8–80% plastic strains to failure, consistent with both the 4% plasticity as well as the decrease of engineering stress with the onset of plastic strain shown in their Fig. 4 [although the 4% elastic strain at 60 Kg/mm$^2$ stress (590 MPa) gives a low apparent modulus of 15 GPa for the specimen]. In general, thin specimens are especially affected by such instabilities once plastic deformation begins. For this reason the yield stress should generally be a more meaningful number than the UTS for comparing tests on specimens with different gauge dimensions. An ASTM standard for testing of foils does exist.[21] However, adherence to the specified dimensions is not always possible due to limitations associated with fabrication.

The average UTS of the large gauge Al/Ti multilayers becomes erratic as bilayer thickness $\Lambda$ decreases (Table I), contrasting with a relatively smooth plateau of the average UTS observed by Lehoczky for Al/Cu multilayers with $\Lambda < 140$ nm. This is believed to be related to the presence of deposition defects and regions of intergranular failure on the generally ductile fracture surfaces of the Al/Ti multilayers (Figs. 6 and 7). The presence of "high imperfection content" in multilayers deposited on low temperature substrates, believed to result from reduced mobility of the depositing atoms, has been noted by Bunshah *et al.*[6] As such, the use of a water-cooled substrate for deposition of the Al/Ti multilayers is believed to be responsible for many of the defects and associated regions of intergranular failure on the fracture surfaces of the tensile specimens. The use of higher substrate temperature or ion beam assisted deposition, though resulting in increased mixing at the Ti/Al interfaces, should reduce this defect population, possibly allowing these materials to more consistently demonstrate the high UTS values exhibited by some of the tensile specimens.

The source of the strain rate dependent plastic strain exhibited by the 90 nm Al/Ti multilayers is unknown, though increased compliance associated with time dependent growth of cracks at defects is a possibility. The higher yield stresses of the small $\Lambda$ specimens (Table I) would be expected to result in less ductile blunting of such cracks, increased crack growth rates, and failure that is more brittle in nature. This shift from ductile to brittle behavior would be consistent with the increased scatter of the UTS at small $\Lambda$, itself typical of high strength materials. The increase of yield stress with decreasing $\Lambda$ is qualitatively, if not quantitatively [Fig. 4(b)], consistent with Ahuja and Frasier's hardness results.[10]

## V. CONCLUDING REMARKS

Al/Ti multilayer specimens exhibited yield stresses that increased with decreasing bilayer thickness over the 90 to 13 nm range of bilayer thicknesses studied. The scatter of the UTS values increased with decreasing bilayer thickness, consistent with the observed increase of the yield stress and associated premature failure at defects in the specimens. In spite of the deposition defects and their effect on the average fracture strength

TABLE II. Comparison of ultimate tensile strengths and specific tensile strengths for Al/Ti multilayers[1] and previously studied multilayer materials[2].

| Material | Average UTS[3] (MPa) | Highest UTS (MPa) | Average density ($g \cdot cm^{-3}$) | Average UTS/density ($MPa \cdot cm^3 \cdot g^{-1}$) | Highest UTS/density ($MPa \cdot cm^3 \cdot g^{-1}$) |
|---|---|---|---|---|---|
| 14 nm (2 : 1 Al : Ti) (single) | 990 ± 97 | 1080 | 3.30 ± 0.05 | 300 ± 34 | 327 |
| 14 nm (2 : 1 Al : Ti) (multi) | 788 ± 28 | 816 | 3.30 ± 0.05 | 239 ± 12 | 247 |
| 13 nm (2 : 1 Al : Ti) | 727 ± 53 | 780 | 3.34 ± 0.02 | 218 ± 17 | 234 |
| 20 nm (16 : 7 Al : Ti) | 581 ± 52 | 656 | 3.25 ± 0.05 | 179 ± 19 | 202 |
| 40 nm (2 : 1 Al : Ti) | 652 ± 59 | 751 | 3.31 ± 0.04 | 197 ± 20 | 227 |
| 90 nm (2 : 1 Al : Ti) | 655 ± 9 | 670 | 3.33 ± 0.04 | 197 ± 5 | 201 |
| 400 nm (1 : 1 Cr : Cu)[15] | 520 | 520 | 8.0 | 65 | 65 |
| 800 nm (1 : 1 Ti : Ni)[15] | 240 | 240 | 6.7 | 36 | 36 |
| 400 nm (1 : 1 Fe : Cu)[6] | 680 | 680 | 8.4 | 81 | 81 |
| 80 nm (1 : 1 Al : Cu)[8] | 733 | NA[4] | 5.8 | 126 | NA |
| 100 nm (1 : 1 Cu : Ni)[6] | 640 | 640 | 8.9 | 72 | 72 |
| 2 nm (1 : 1 Cu : Ni)[5] | 1040 | 1040 | 8.9 | 117 | 117 |
| 2.6 nm (1 : 1 Cu : NiFe)[16 5] | 1330 | 1330 | 8.8 | 151 | 151 |
| 20 nm (1 : 9 Cu : Ni)[4] | 1900 | NA | 8.9 | 213 | NA |
| 75 nm (1 : 9 Cu : Ni)[17] | 1116 | 1116 | 8.9 | 125 | 125 |
| 100 nm (1 : 9 Cu : Ni)[18] | 1269 | 1397 | 8.9 | 143 | 157 |
| 200 nm (1 : 1 Cu : Ni)[3] | 770[6] | 1080 | 8.9 | 87 | 121 |
| 2 $\mu$m (2 : 1 W : Ta)[19 7] | 450 | 450 | 18.4 | 24 | 24 |
| Mo : W (multiscalar)[20 8] | 132 | NA | 10.4 | 12.6 | NA |

[1]Properties of the Al/Ti multilayers are from Table I. [2]The listed UTS for other studies is that of the strongest bilayer thickness and composition. [3]Where only a single specimen was tested, the value is listed as both highest UTS and average UTS. [4]Value not available (NA). [5]Their "supermodulus" of 603 GPa is assumed to reflect strain rather than stress measurement error. [6]The average UTS is given for retesting of broken specimens; the average UTS for the original testing was 550 MPa. [7]The value given corresponds to a stress rupture time of 8.2 h at 1093 °C. [8]Multilayers were composed of multiple repetitions of 29 × (4 nm Mo/4 nm W) + 5 $\mu$m of Mo.

of the materials studied, the highest ultimate tensile strengths obtained are similar to those of other multilayer materials. The specific strength (UTS divided by density) of the strongest Al/Ti multilayers is significantly higher than that of all other published multilayer systems of which the authors are aware. The opportunity to improve these materials, e.g., by adjusting deposition conditions to reduce the defect population, is being pursued. The use of intentional alloying in vapor deposition is being considered for future work.

## ACKNOWLEDGMENTS

D. Josell and D. Shechtman acknowledge the support of the U.S.–Israel Binational Science Foundation. D. van Heerden acknowledges the support of the United States Air Force.

## REFERENCES

1. G. S. Was and T. Foecke, Thin Solid Films **286**, 1 (1996).
2. S. A. Barnett, in *Physics of Thin Films: Mechanic and Dielectric Properties*, edited by M. H. Francombe and J. L. Vossen (Academic Press, San Diego, 1993), pp. 2–27.
3. C. A. O. Henning, F. W. Boswell, and J. M. Corbett, Acta Metall. **23**, 193 (1975).
4. S. Menezes and D. P. Anderson, J. Electrochem. Soc. **137**, 440 (1990).
5. D. Baral, J. B. Ketterson, and J. E. Hilliard, J. Appl. Phys. **57**, 1076 (1985).
6. R. F. Bunshah, R. Nimmagadda, H. J. Doerr, B. A. Movchan, N. I. Grechanuk, and E. V. Dabizha, Thin Solid Films **72**, 261 (1980).
7. S. Rao, P. M. Hazzledine, and D. M. Dimiduk, in *Grain-Size and Mechanical Properties—Fundamentals and Applications*, edited by N. J. Grant, R. W. Armstrong, M. A. Otooni, and K. Ishizaki (Mater. Res. Soc. Symp. Proc. **362**, Pittsburgh, PA, 1995), pp. 67–77.
8. S. L. Lehoczky, J. Appl. Phys. **49**, 5479 (1978).
9. S. L. Lehoczky, Phys. Rev. Lett. **41**, 1814 (1978).
10. R. Ahuja and J. L. Fraser, J. Electron. Mater. **23**, 1027 (1994).
11. D. T. Read and J. W. Dally, AMD Vol. 187, *Mechanics and Materials for Electronic Packaging: Vol. 2: Thermal and Mechanical Behavior and Modeling*, (ASME, 1994), p. 41.
12. D. van Heerden, D. Josell, and D. Shechtman, Acta Mater. **44**, 297 (1996).
13. D. Shechtman, D. van Heerden, and D. Josell, Mater. Lett. **20**, 329 (1994).
14. *ASM Metals Reference Book*, 2nd ed. (American Society for Metals, Metals Park, OH, 1983).
15. R. F. Bunshah, R. Nimmagadda, H. J. Doerr, B. A. Movchan, N. I. Grechanuk, and G. G. Didkin, Thin Solid Films **112**, 227 (1984).
16. A. Jankowski and T. Tsakalakos, J. Appl. Phys. **57**, 1835 (1985).
17. D. M. Tench and J. T. White, J. Electrochem. Soc. **138**, 3757 (1991).
18. D. Tench and J. White, Metall. Trans. A **15A**, 2039 (1984).
19. C. A. Hoffman and J. W. Weeton, Metall. Trans. **5**, 309 (1974).
20. M. Vill, D. P. Adams, S. M. Yalisove, and M. C. Bilello, Acta Metall. Mater. **43**, 427 (1995).
21. *1994 Annual Book of ASTM Standards Vol. 3.01, Standard Test Methods of Tension Testing of Metallic Foils, Designation E 345-93*, (ASTM, Philadelphia, 1994), pp. 376–380.